Developmental Cell, Volume *46*

Supplemental Information

Combinatorial Contact Cues Specify Cell Division Orientation by Directing Cortical Myosin Flows

Kenji Sugioka and Bruce Bowerman

Figure S1 (Sugioka, Bowerman)

Figure S1. Related to Figure 2. Related to Figure 2. Orientations of mouse third embryonic division require zona-pellucida.
Mouse 4-cell stage embryos after live-imaging. With or without zona-pellucida removal, all AB cells underwent parallel division. However, 25% of zona-free CD divisions were perpendicular to the contact plane. Arrow indicates CD cell division axis. Scale bars = 10 μm.

Figure S2 (Sugioka, Bowerman)

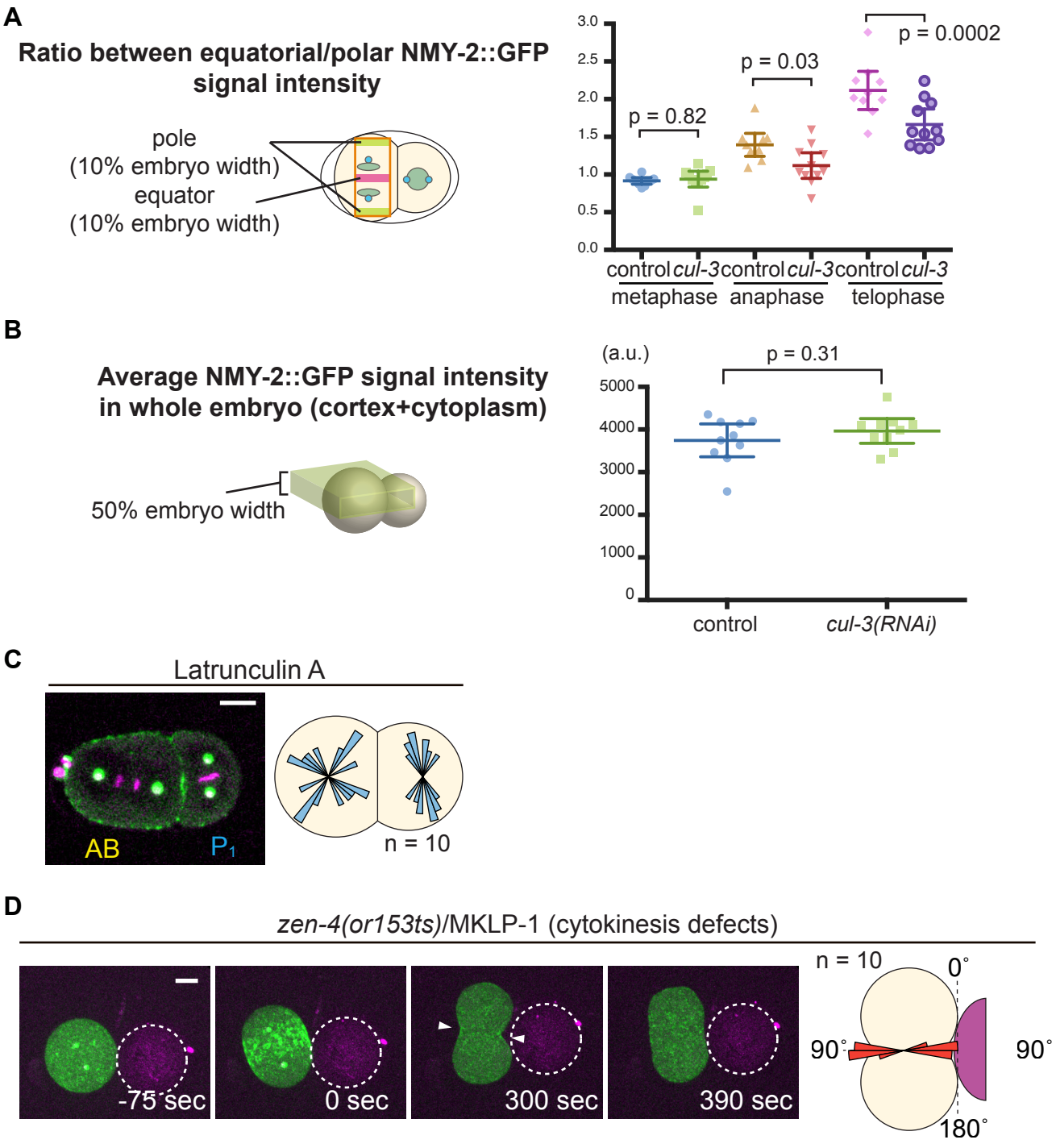

Figure S2. Related to Figure 3. Oriented AB division requires actomyosin activity but not cytokinesis. (A) Myosin spatial distribution during AB cell division. Ratios of signal intensities of polar and equatorial regions of 10% embryo width were calculated from maximum projection images, as in left schematics. P-values were calculated by one-way ANOVA with Holm-Sidak's multiple comparison test. (B) Amount of NMY2::GFP signal was not altered by *cul-3(RNAi)*. Average signal intensity of NMY-2::GFP in AB cell was calculated using the Z projection images (sum slices) that included 50% volume of embryo from cell surface to middle of the embryos. P-values were calculated by Welch's t-test. (C) Abnormal AB division axes after treatment with latrunculin A. The distribution of AB and P_1 mitotic spindle orientation is shown on the right. (B) Physical contact-dependent oriented AB division in cytokinesis-defective mutant background. Myosin (green), centrosomes (green), bead (magenta; dotted white lines), histones (magenta), and cleavage furrow position (arrowheads) are shown. The distribution of cleavage furrow orientation is shown on the right. Scale bars = 10 μm.

Figure S3 (Sugioka, Bowerman)

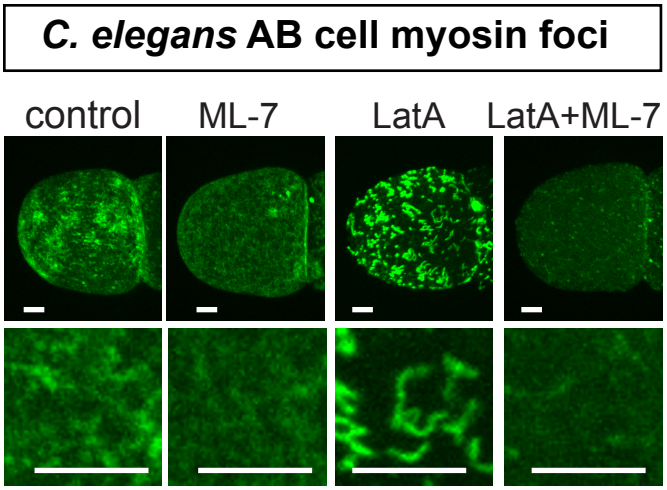

Figure S3, Related to Figure 4. Myosin foci formation is inhibited by ML-7 treatment. Myosin foci on the AB cell cortex during late anaphase. Bottom panels are magnified views. Myosin (green) is shown. Scale bars = 10 μm.

Figure S4 (Sugioka, Bowerman)

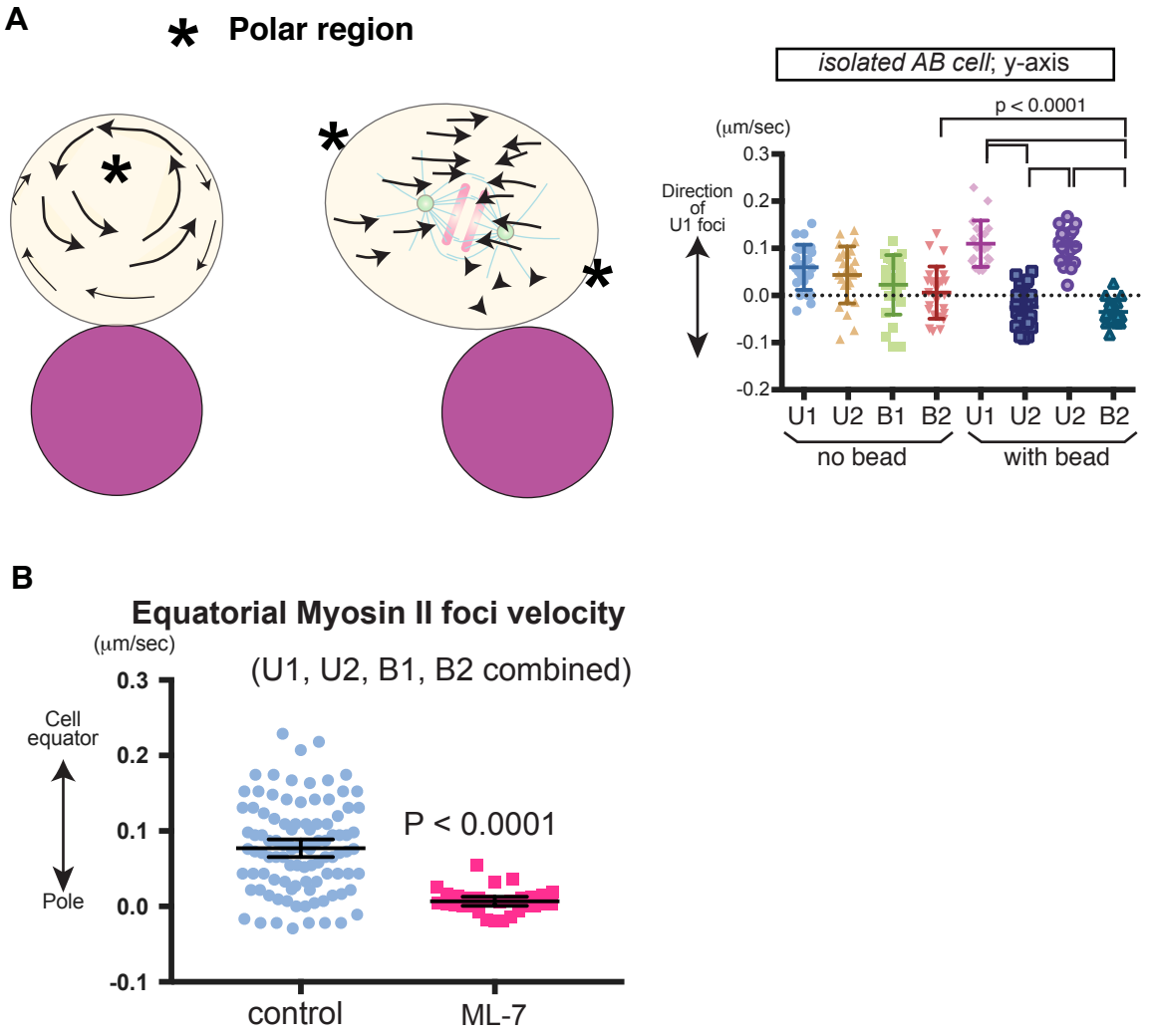

Figure S4, Related to Figure 5. Myosin flow is limited by cell contact and ML-7 inhibitor.
(A) Myosin foci movements summarized from the data in Fig. 5. Right graph show Y-axis myosin flow velocities in isolated AB cells. (B) Myosin foci velocities (x-axis) of total AB cell region combined for intact embryos (control) and ML-7treated embryos. P-values in (A) were calculated by the one-way ANOVA with Holm-Sidak's multiple comparison test and in (B) was calculated by the Welch's t-test.

Figure S5 (Sugioka, Bowerman)

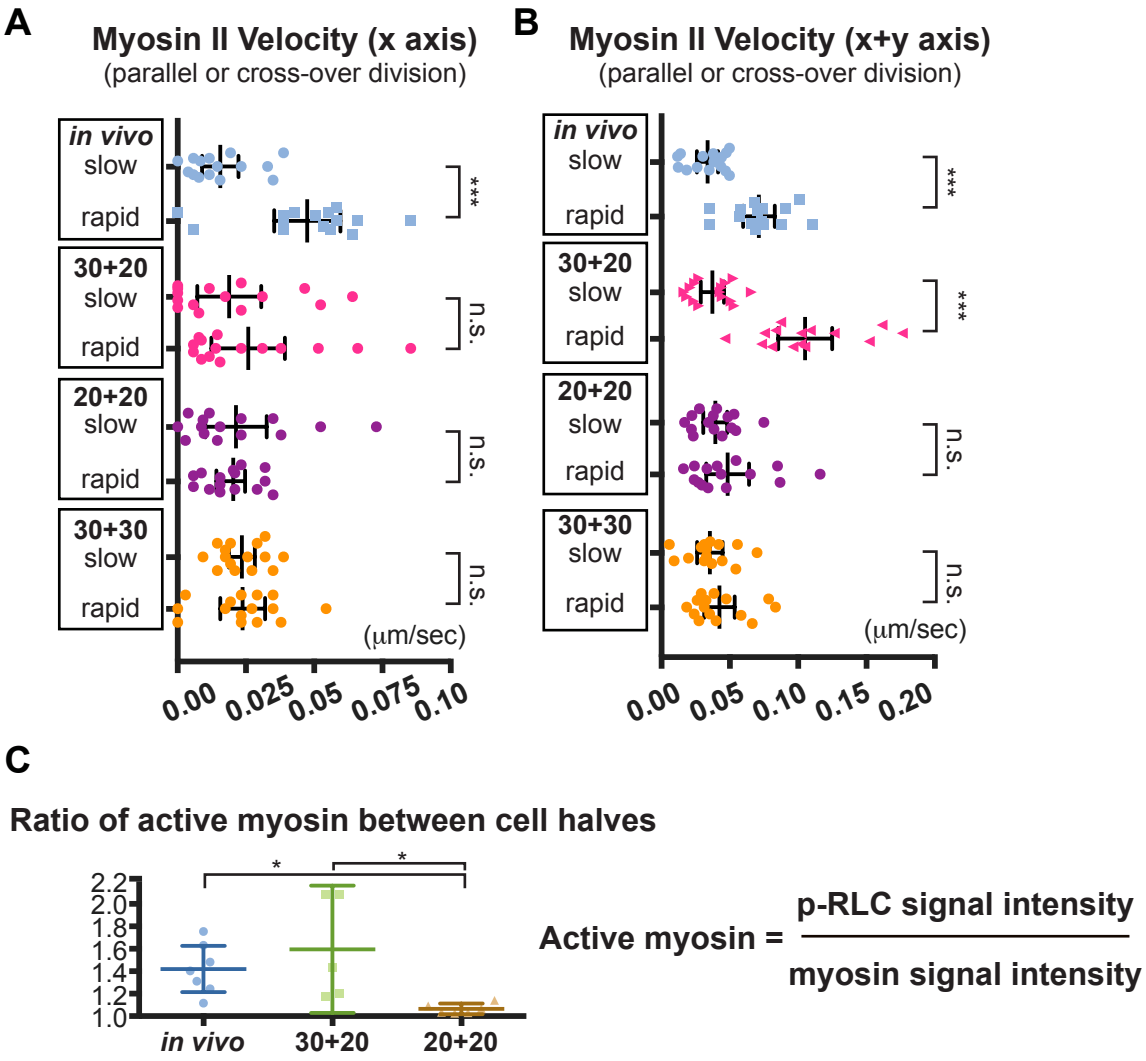

Figure S5. Related to Figure 6. Myosin flow velocities and activity during ABa division.
(A, B) Myosin flow velocities in ABa cell of x-axis (A) and x+y axis (B) in the indicated experiments are shown.
(C) Ratio of active myosin between dividing cell halves. Active myosin levels were calculated as in the right equation. P values were calculated by one-way ANOVA with Holm-Sidak's multiple comparisons test.
*P < 0.05, ***P < 0.0001; n.s., not significant (P > 0.05).

Figure S6 (Sugioka, Bowerman)

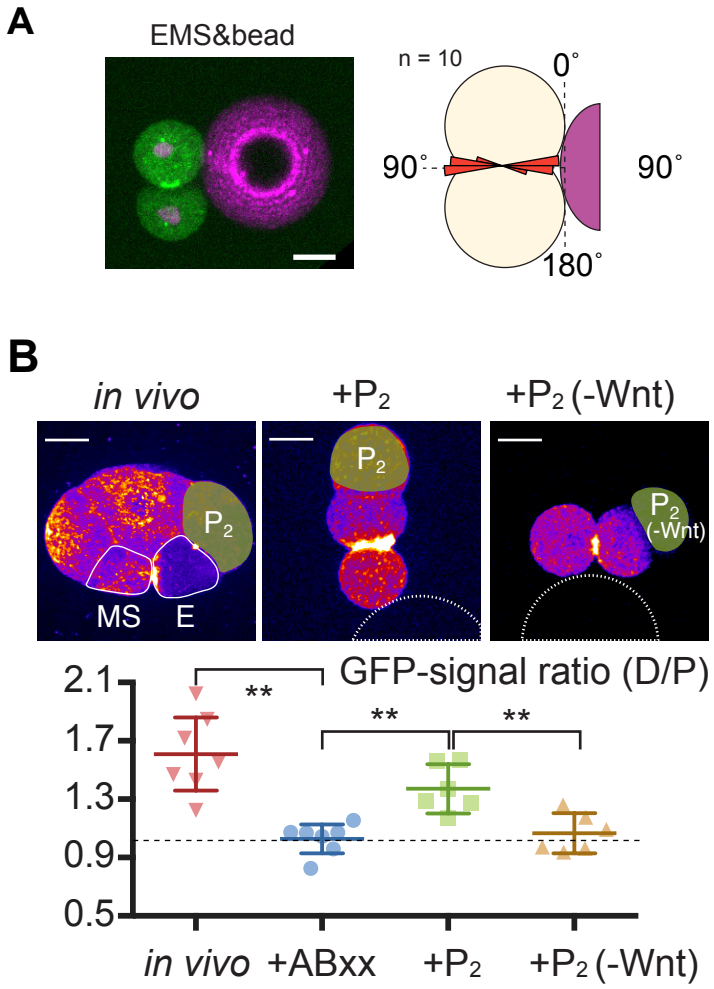

Figure S6. Related to Figure 7. Response to physical contact and myosin distribution during EMS division. (A) EMS division axis in response to physical contact. Distribution of cleavage furrow orientation is shown on the right. (B) Polarized myosin localization in the presence of Wnt signal. Heat maps of myosin GFP signal intensity are shown. White solid lines in the figure of in vivo indicate EMS cells and white dotted lines in the middle and right panels indicate beads. P values were calculated by one-way ANOVA with Holm-Sidak's multiple comparisons test. *P < 0.05, **P < 0.01, ***P < 0.0001; n.s., not significant (P > 0.05). Scale bars = 10 μm.

Figure S7 (Sugioka, Bowerman)

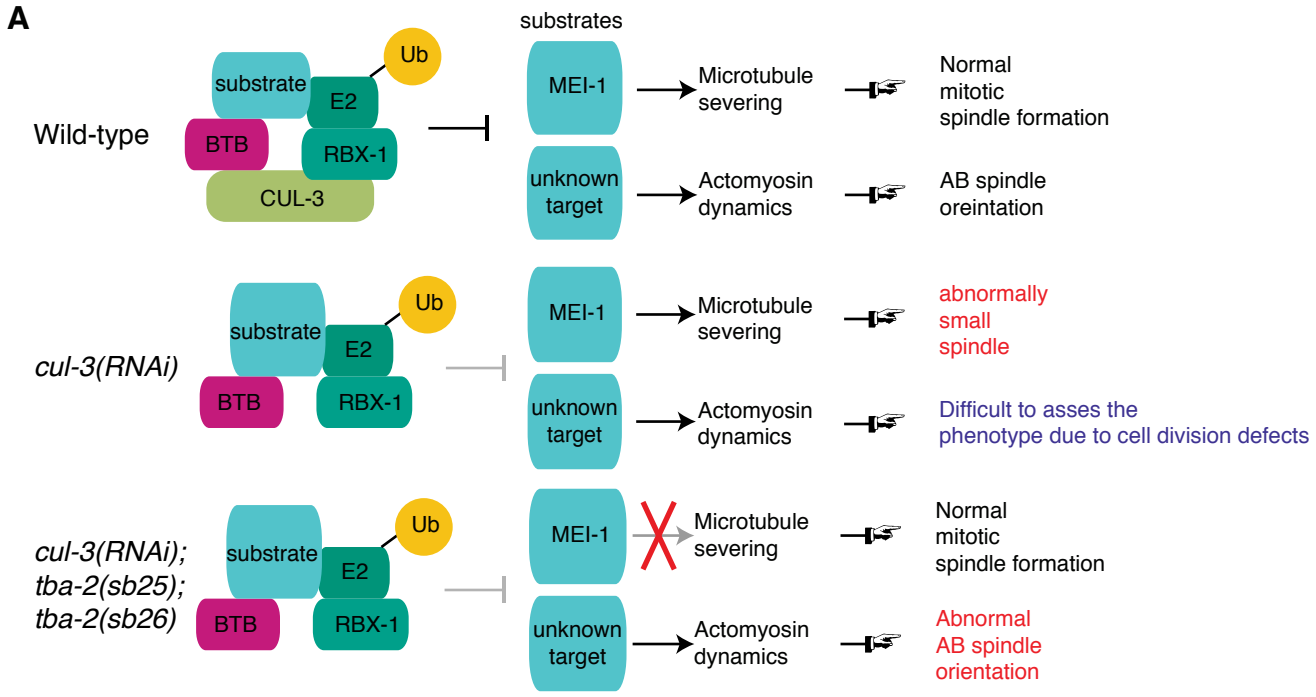

B

	tba-2(sb25);tbb-2(sb26)		
	control(RNAi)	*cul-3(RNAi)*	*mei-1(ct46)*
viability	98.3% (n = 289)	0% (n = 98)	99.0% (n = 707)

C AB cleavage furrow orientation

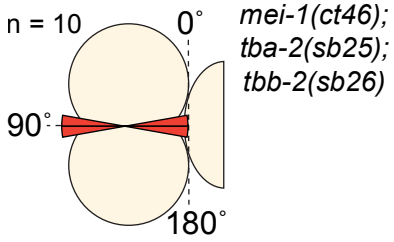

Figure S7. Related to the STAR Methods. Genetic backgrounds used to assess MEI-1-independent *cul-3* phenotype.
(A) Schematic illustrations of genetic backgrounds used in this study. CUL-3/Cullin forms an E3 ubiquitin ligase complex with BTB protein, RBX-1 and E2 enzyme to ubiquitylate substrate proteins. The CUL-3 E3 ligase regulates the degradation of the meiosis-specific microtubule-severing protein MEI-1 during the oocyte-to-embryo transition to allow formation of a normal mitotic spindle. Upon *cul-3* knock-down or in degradation-defective *mei-1(ct46)* mutants, ectopic MEI-1 protein activity during mitosis causes the formation of abnormally small spindles with short microtubules (middle panel). However, when *tba-2(sb25)* and *tbb-2(sb26)* mutations are introduced (α-tubulin and β-tubulin alleles, respectively), microtubules become resistant to ectopic MEI-1 protein activity (Lu and Mains, 2005) and normal mitotic spindle formation is restored (bottom panel). In *cul-3(RNAi)* embryos, AB spindle orientation is defective in the *tba-2(sb25);tbb-2(sb26)* background, suggesting that this phenotype results from a failure to degrade unknown target(s). (B, C) Viability and AB cleavage furrow orientation after *cul-3* knockdown are independent of ectopic MEI-1 function. Eggs were laid by adult worms for around 6 h and hatched and dead embryos were counted to assess viability in B. Note that the degradation-defective mutant *mei-1(ct46)* showed 0% viability in a wild-type background (Lu and Mains, 2005), which was completely rescued to wild-type levels in the *tba-2(sb25);tbb-2(sb26)* background (B). Cleavage furrow orientations of AB division in *mei-1(ct46); tba-2(sb25); tbb-2(sb26)* were normal (C).